IMPACT OF BOUNDARY-LAYER CUTTING AND FLOW CONDITIONING ON FREE-SURFACE BEHAVIOR IN TURBULENT LIQUID SHEETS

S.G. Durbin[†], M. Yoda, and S.I. Abdel-Khalik

G. Woodruff School of Mechanical Engineering
Georgia Institute of Technology
Atlanta, GA 30332-0405 USA
[†]*(404) 385-1891   gte397r@mail.gatech.edu*

The HYLIFE-II conceptual design uses arrays of high-speed oscillating and stationary slab jets, or turbulent liquid sheets, to protect the reactor chamber first walls. A major issue in thick liquid protection is the hydrodynamic source term due to the primary turbulent breakup of the protective slab jets. During turbulent breakup, drops are continuously ejected from the surface of turbulent liquid sheets and convected into the interior of the cavity, where they can interfere with driver propagation and target injection. Experimental data for vertical turbulent sheets of water issuing downwards from nozzles of thickness (small dimension) $\delta = 1$ cm into ambient air are compared with empirical correlations at a nearly prototypical Reynolds number $Re = 1.2 \times 10^5$. A simple collection technique was used to estimate the amount of mass ejected from the jet surface. The effectiveness of boundary-layer cutting at various "depths" into the flow to reduce the source term and improve surface smoothness was evaluated. In all cases boundary-layer cutting was implemented immediately downstream of the nozzle exit. Planar laser-induced fluorescence (PLIF) was used to visualize the free-surface geometry of the liquid sheet in the near-field region up to 25δ downstream of the nozzle exit. Large-scale structures at the edges of the sheet, typically observed for $Re < 5.0 \times 10^4$, reappeared at $Re = 1.2 \times 10^5$ for sheets with boundary-layer cutting. The results indicate that boundary-layer cutting can be used to suppress drop formation, i.e. the hydrodynamic source term, for a well-conditioned jet but is not a substitute for well-designed flow conditioning.

I. INTRODUCTION

Thick liquid protection is potentially an innovative solution for first wall protection and heat removal for inertial fusion energy (IFE) reactor chambers. The High-Yield Lithium-Injection Fusion Energy (HYLIFE-II) IFE power plant design proposed using slab jets, or liquid sheets, of molten Flibe (Li_2BeF_4) for cooling and attenuation of damaging radiation and target debris.[1] However, jets in the range of interest for HYLIFE-II are susceptible to primary turbulent breakup[2,3], or breakup (atomization) involving only internal forces such as turbulent or inertial forces, or forces due to vorticity. The fluid ejected along the free surface of the jet due to turbulent breakup is here called the "hydrodynamic source term." Previous work on turbulent annular liquid sheets and round jets have proposed correlations for estimating the onset of and mass flux due to primary breakup.[3] These correlations were developed for jet initial conditions corresponding to unconditioned, fully-developed turbulent pipe flow.

A number of studies have shown that turbulent breakup is suppressed in round jets with nearly uniform initial velocity profiles.[4,5] Wu *et al.* used a knife-edge to remove the boundary layer (BL) from the flow near the nozzle exit. The boundary-layer cutter had a relatively short reattachment length, preventing substantial growth of a new BL. Our group has previously demonstrated that boundary-layer cutting can be used to eliminate breakup (within experimental error) for turbulent liquid sheets.[6]

In our previous study, a relatively large amount of BL cutting to a depth of 0.25 mm from the inner surface of the nozzle, corresponding to removing 1.5% of the total mass flux $\dot{m}_{fl}$, was used. BL cutting was found to be effective at suppressing breakup in only a "well-conditioned" flow. This subsequent work focuses upon optimizing the amount of BL cutting (in terms of the fraction of total mass flux removed) to suppress turbulent breakup while minimizing the amount of "cut" fluid, and exploring how changes in flow conditioner design impact the effectiveness of BL cutting.

Liquid sheets of water issuing vertically downwards into ambient air were studied experimentally in the near-field $x/\delta \leq 25$. The coordinate system used here has its origin at the center of the nozzle exit, with x along the flow direction, and y and z along the long and short dimensions of the nozzle, respectively. The Reynolds and Weber numbers are $Re = U_o\delta/\nu = 1.2\times10^5$ and $We = \rho_L U_o^2 \delta/\sigma = 1.9\times10^4$, respectively. Here, U_o is the average jet speed and δ the z-dimension of the jet at the nozzle exit. The liquid kinematic viscosity, liquid density

and liquid-air surface tension are denoted by ν, ρ_L and σ, respectively. The Re and We for these investigations are about one-half and one-fifth of the HYLIFE-II prototypical values. The effectiveness of BL cutting at levels ranging from 0–1.9% of $\dot{m}_{\text{fl}}$, were evaluated for a standard flow conditioner design and an otherwise identical design without the fine screen.

II. TURBULENT BREAKUP CORRELATIONS

The hydrodynamic source term, measured by a simple mass collection technique, is compared to published correlations for turbulent primary breakup of liquid jets based upon pulsed shadowgraphy and holography data.[3] These correlations were developed for round and annular jets with fully-developed turbulent velocity profiles at the nozzle exit with neither flow conditioning nor a contracting nozzle upstream.

Using pulsed shadowgraphy to measure the streamwise and cross-stream droplet velocity components $\tilde{u}$ and $\tilde{v}$, respectively, Sallam *et. al.* reported values of $\tilde{u}/U_o = 0.78$ and $\tilde{v}/U_o \leq 0.089$. They also concluded that $\tilde{v}_r$, the cross-stream velocity of the droplets measured with respect to the free surface, was proportional to the average speed at the nozzle exit, with $\tilde{v}_r/U_o = 0.04$.

The mass flux of droplets relative to the liquid surface due to turbulent primary breakup is denoted as G [kg/(m^2·s)]. The droplet mass flux was measured directly by single-pulse holography and normalized to give the surface efficiency factor $\varepsilon \equiv G/(\rho_L \tilde{v}_r)$. A 100% efficiency factor therefore corresponds to droplets emitted from the entire jet free surface. Based on measurements of G and $\tilde{v}_r$, the surface efficiency factor is then[3]

$$\varepsilon = \frac{0.272x}{d_h \sqrt{We_d}} \qquad (1)$$

where d_h is the hydraulic diameter of the jet and We_d is the Weber number based upon d_h. Eq. (1) is valid for We_d = 235–270,000.

III. APPARATUS AND PROCEDURES

III. A. Flow Loop

As detailed elsewhere,[6,7] water at 24°C was pumped through the flow conditioning section and contracting nozzle to form the liquid sheet in the open test section in the recirculating flow loop. The flow conditioner (Fig. 1) consisted of a stainless steel (SS) perforated plate (50% open area ratio, 4.8 mm diameter staggered holes), PP,

followed by a 2.5 cm section of polycarbonate (circular cells of diameter 0.32 cm), HC 3.9 cm farther downstream. In the "standard" flow conditioner configuration, a SS fine screen (37.1% open area and 0.33 mm wire diameter), FS, was placed 0.5 cm downstream of the HC. In the "no screen" configuration, the FS was removed to evaluate the effectiveness of BL cutting for different flow conditioner configurations.
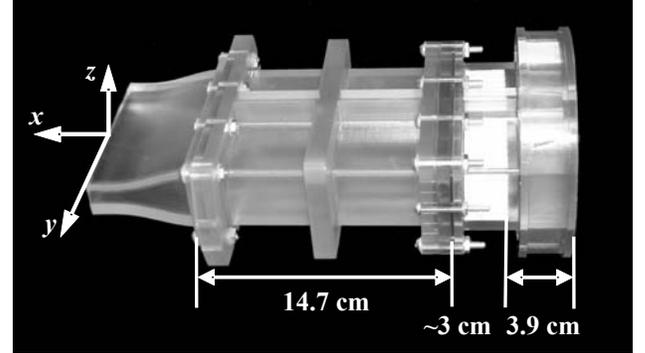

Fig. 1. Flow conditioner / nozzle assembly.

The nozzle downstream of the flow conditioner was a 5th order polynomial contraction with an area contraction ratio of 3 and exit y- and z- dimensions of $\delta = 1$ cm and $W_o = 10$ cm, respectively. The nozzle exit had a slight contraction with a slope of 4°.[7]
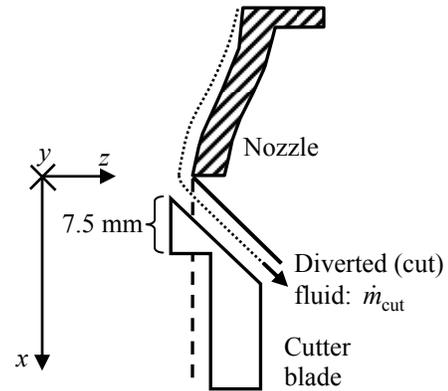

Fig. 2. Schematic of BL cutter (enclosure around cutter blade not shown).

Figure 2 shows the BL cutter and its placement with respect to the nozzle. The cutter used in this study, which was mounted independently from the nozzle, was used to remove fluid from only one face along the y-axis of the jet just downstream of the nozzle exit at $x = 0.076$ cm. The cutter assembly was supported on a linear stage that enabled fine adjustments along the z-direction. The cutter blade, machined from aluminum, had a reattachment length of 7.5 mm and a width (y-extent) of 12 cm that

extended 1 cm beyond the jet on both sides. A range of different levels of BL cutting ranging from $\dot{m}_{cut} / \dot{m}_{fl} = 0$–1.9% ($\dot{m}_{cut}$ is the diverted mass flowrate)—were evaluated.

III. B. Measurement of Ejected Mass

The amount of drops ejected from the free surface was measured by collecting fluid in an array of square cuvettes.[6] A row of five square cuvettes (inner dimension 1 cm) centered with respect to the y-axis were placed just beyond the free surface at the furthest downstream location of $x/\delta = 25$ (Fig. 3). The cuvette standoff distance Δz_s was measured from the nearest inner wall of the nozzle, or the nominal jet free surface. The row of cuvettes were tilted towards the free-surface at 6.5° with respect to the vertical; this tilt was based upon drop trajectories predicted by the correlations described in the previous section. The cuvettes were weighed on a digital scale to ±1 mg accuracy before and after each 30–60 minute collection period; the resultant mass difference is then an estimate of the mass of drops ejected from the free surface.
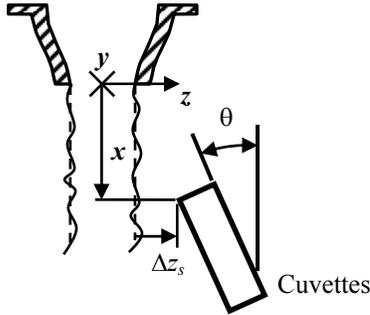

Fig. 3. Sketch of mass collection setup. The cuvettes are brought to a distance Δz_s from the nominal free surface (dashed line) at $\theta \approx 6.5°$.

The experimental mass flux G_{exp} is then the collected mass divided by the collection time and total cuvette cross-sectional area of 5 cm². The equivalent average number density N was then defined as

$$N = \frac{\rho_{eff} N_A}{M}, \quad \text{where} \quad \rho_{eff} = \frac{G_{exp}}{\sqrt{\tilde{u}^2 + \tilde{v}^2}} \qquad (2)$$

Here, ρ_{eff} is the effective line density and N_A and M are Avogadro's number and molecular weight, respectively. This number density is provided to evaluate whether these flows are compatible with the requirements for a specific driver or target designs.

III. C. Free Surface Visualization

Planar laser-induced fluorescence (PLIF) was used to visualize the free surface of the liquid sheet.[7] The water in the flow loop contained 26 mg/L disodium fluorescein, a dye that fluoresces in the yellow-green when illuminated at 488 nm. This relatively high dye concentration was chosen so that most of the illuminating light was absorbed within a few millimeters of the free surface (cf. Fig. 5a). Refraction of spurious fluorescence that could interfere with imaging the flow free surface was thus minimized. The flow was illuminated at various x-locations by a ~0.2 cm thick 488 nm laser light sheet with a net power of about 0.2 W; the sheet was formed from a multiline argon-ion laser beam passed through a notch filter (Edmund Scientific NT30-907).

The free surface was imaged as the interface between fluorescing water and non-fluorescing air by an obliquely mounted B/W CCD camera (Kodak Model ES 1.0) from below at 30 Hz with a close-focusing macro video lens (Navitar Zoom 7000) (Fig. 4). A high-pass wavelength filter (Sunpak Yellow-8) with a cut-off frequency of 500 nm was mounted to the camera lens to ensure that the camera imaged only the longer-wavelength fluorescence.
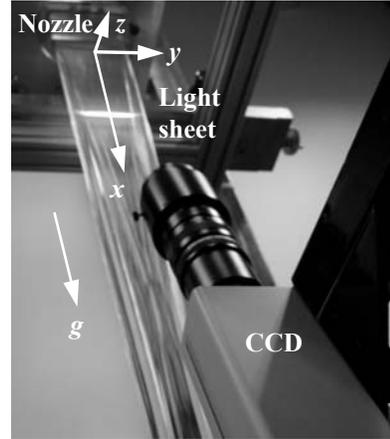

Fig. 4. PLIF experimental setup.

The field of view for each image is about 3.0 cm (y) × 3.0 cm (z). One side (i.e., the entire y-extent) of the flow is then visualized by overlapping 4–5 segments, with each segment comprised of 134 consecutive images with an exposure of $\tau \equiv \delta / U_o$. The whole side then spans at least 5200τ. Individual images were stored as 8-bit 1008 × 1008 bitmaps on a PC HD using digital video recording software (Video Savant 3.0).

The free surface is found in each image using a threshold-based edge detection algorithm written in MATLAB (Fig. 5). The grayscale threshold value was chosen based upon a histogram of grayscale vs. number of pixels for the entire dataset. If M_p is the number of pixels

at the maximum of the background peak, the threshold grayscale is then the smallest grayscale above the background that contains at least 1% of M_p pixels. For every segment, the free-surface locations are determined for each of 134 thresholded images using a standard edge detection scheme and are used to calculate the average z-location of the free surface and its standard deviation. This standard deviation was spatially averaged over the central 75% of the flow ($|y/W_o| \le 0.375$) to obtain σ_z.
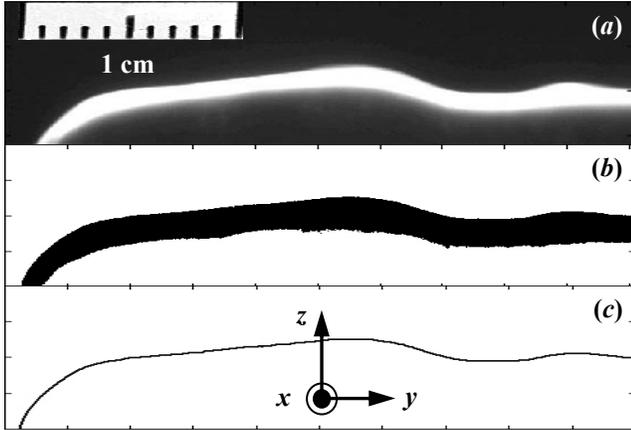

Fig. 5. Illustration of the process used to find the liquid sheet free surface: (*a*) Raw PLIF image; (*b*) Thresholded image; and (*c*) Free surface obtained by edge detection.

Each segment of the free surface has a slight overlap with neighboring segments. In all cases, the free surface fluctuations in this overlap region are taken to be those calculated for the left segment. The extent of the overlap region is known from a reference scale imaged in each frame. No significant discontinuities were observed using this procedure, since the central portion of the jet exhibits nearly constant surface fluctuations.

IV. RESULTS

IV. A. PLIF Experiments

Figure 6 shows σ_z / δ averaged over the central 75% of the flow ($|y/W_o| < 0.375$) as a function of x / δ for the standard (black) and no screen (grey symbols) flow conditioner configurations at $\dot{m}_{cut} / \dot{m}_{fl} = 0\%$ (■), 1.0% (◆), and 1.9% (▲). As expected, BL cutting significantly reduces the standard deviation of the free surface. However, "cutting" more fluid has little discernible impact upon σ_z; the results at $\dot{m}_{cut} / \dot{m}_{fl} = 1.0\%$ and 1.9% are virtually identical. Removing 1.9% of the overall mass flux from the surface reduced σ_z on average by about 33% and 10% for the standard and no screen configurations, respectively. In the absence of BL

cutting, the standard deviation of the standard configuration was about 67% lower than that for the no screen configuration. BL cutting clearly reduces surface ripple, but the fine screen has a larger overall impact on free-surface smoothness.
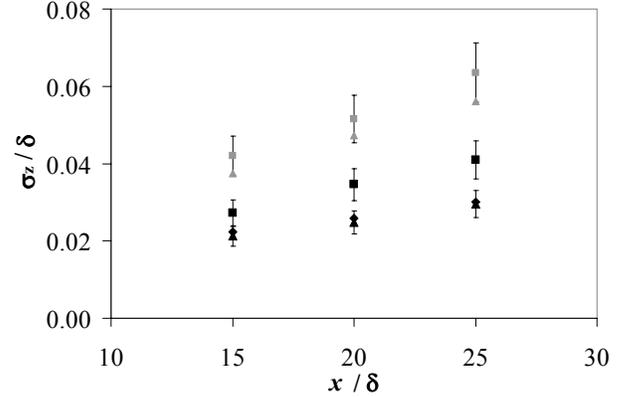

Fig. 6. σ_z / δ vs. x / δ for standard (black) and no screen (grey) flow conditioning configurations at $\dot{m}_{cut} / \dot{m}_{fl} = 0.0\%$ (■), 1.0% (◆), and 1.9% (▲). The error bars in this and the following Figure represent 95% confidence intervals.
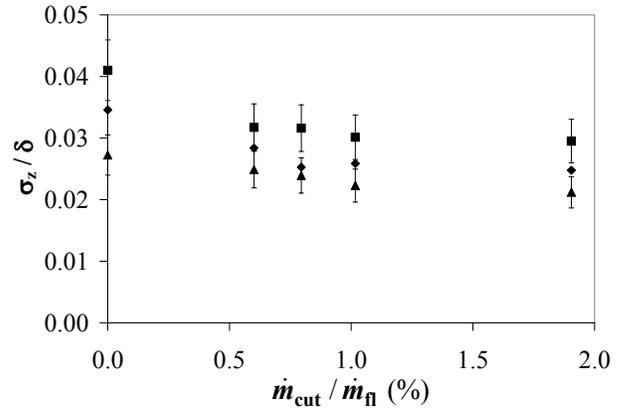

Fig. 7. σ_z / δ *vs.* $\dot{m}_{cut} / \dot{m}_{fl}$ for standard flow conditioning at $x / \delta = 15$ (▲), 20 (◆), and 25 (■).

Figure 7 shows the effects of different levels of BL cutting on free-surface fluctuations for the standard flow configuration at $x / \delta = 15$ (▲), 20 (◆), and 25 (■). Surface ripple decreases at all downstream locations as $\dot{m}_{cut} / \dot{m}_{fl}$ increases; σ_z is reduced significantly even at BL cutting levels as low as $\dot{m}_{cut} / \dot{m}_{fl} = 0.6\%$. Increasing $\dot{m}_{cut} / \dot{m}_{fl}$ provides diminishing improvements in surface smoothness.

BL cutting also alters the average free-surface geometry in turbulent liquid sheets, introducing protrusions near the edges of the flow (Fig. 8). Although

the entire "uncut" free surface at $x/\delta = 25$ lies well within the z-extent of the nozzle (Fig. 8a), the protrusions extend out to the nozzle while the rest of the flow moves even farther away from the nozzle walls (Figs. 8b–c). These end effects may be due to fluid being removed from only one side of the jet, but they clearly demonstrate the sensitivity of this flow to initial conditions. Though not shown here, the y-extent of the "cut" jet in both cases was less than that for the "uncut" flow at all downstream locations; at $x/\delta = 25$, this difference in the y-dimension was about 0.6 cm at $\dot{m}_{cut}/\dot{m}_{fl} = 1.9\%$.
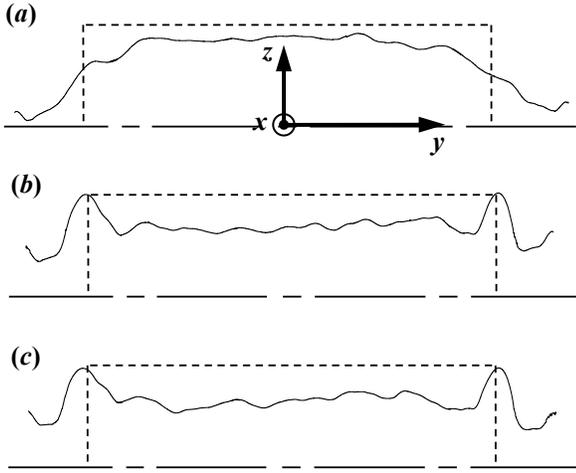

Fig. 8. Average free-surface position at $x/\delta = 25$ for a turbulent liquid sheet with standard flow conditioning at $\dot{m}_{cut}/\dot{m}_{fl} = 0.0\%$ (a); 1.0% (b); and 1.9% (c). The inner walls of the nozzle exit are indicated by the dashed outline; flow is out of the page. Note that the vertical (y) axis is shown at 5× magnification.
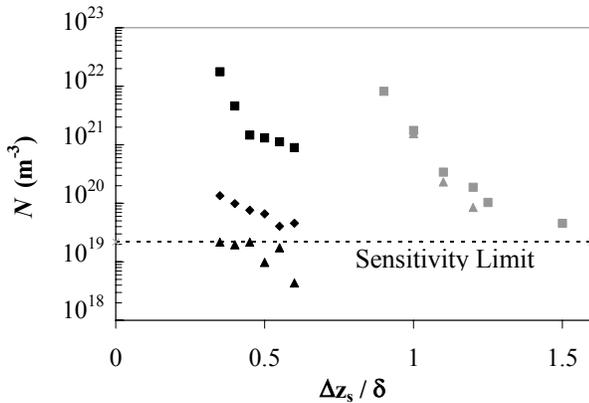
IV. B. Mass Collection Experiments

Fig. 9. Equivalent number density *vs.* $\Delta z_s/\delta$ for standard (black) and no screen (grey) configurations at $\dot{m}_{cut}/\dot{m}_{fl} = 0.0\%$ (■), 1.0% (♦), and 1.9% (▲).

Figure 9 shows equivalent number density as a function of cuvette standoff for standard (black) and no screen (grey symbols) flow conditioning configurations with BL cutting at $\dot{m}_{cut}/\dot{m}_{fl} = 0.0\%$ (■), 1.0% (♦), and 1.9% (▲) at $x/\delta = 25$. The density of drops due to turbulent breakup at the jet free surface increases as Δz_s decreases. Not surprisingly, there are more drops near the source of breakup, namely the jet surface. Note that any measurement below the sensitivity limit indicates a collected mass of zero within experimental error. Secondary effects such as aerodynamic shear, drop re-entrainment, and evaporation limit the spatial distances over which drops can be detected or collected. Approaching the jet, N should therefore increase from zero at a sufficiently large standoff value with a sharp increase as the free surface.

BL cutting reduces the hydrodynamic source term; a marked reduction in breakup is already observed for the standard configuration at a cut rate of 1.0% over all standoff distances. Moreover, breakup is completely suppressed at $\dot{m}_{cut}/\dot{m}_{fl} = 1.9\%$. For the no screen configuration, breakup is observed farther from the free surface. In addition, BL cutting appears to have less impact on the no screen cases, with smaller reductions in N compared with the standard configuration cases. The dominant impact of the fine screen seen here is consistent with the trends observed in the PLIF data; in all cases, the (absence of the) fine screen has a much more significant impact upon jet quality than BL cutting.

The breakup correlations were applied to a turbulent liquid sheet matching the experimental Weber number. Based upon these results, flow conditioning and a contracting nozzle already reduce the mass flux by 3–5 orders of magnitude. Since the experimental conditions in these studies are not identical to those used to establish the correlations, reductions in breakup with respect to the correlations should be considered qualitative. Nevertheless, this discrepancy again demonstrates the sensitivity of these types of flows to initial conditions.

V. CONCLUSIONS

Primary turbulent breakup of liquid sheets at $Re = 1.2\times10^5$ and $We = 1.9\times10^4$ can be suppressed with appropriate combinations of flow conditioning upstream of and boundary-layer cutting downstream of the nozzle. Breakup is completely eliminated (within experimental error) at $\dot{m}_{cut}/\dot{m}_{fl} = 1.9\%$, but the free-surface fluctuations are similar at a given downstream location for $\dot{m}_{cut}/\dot{m}_{fl} > 1.0\%$. The (presence or absence of a) fine screen in the flow conditioner is the dominant factor influencing free-surface smoothness, with the average standard deviation of the free-surface position without a

fine screen 1.5 times that with a fine screen. The inability of BL cutting to suppress this additional surface ripple may be due to a large central disturbance in the z-component of velocity fluctuations that extends into the center of the flow, beyond the range of the cutter blade.[9] BL cutting can be used on a "well-conditioned" liquid sheet to eliminate the hydrodynamic source term, but it does not appear to be capable of eliminating breakup without well-designed flow conditioning.

Primary turbulent breakup in prototypical flows at the much higher Weber number of 10^5 will be comparable based upon the correlations, since Eq. (1) and the definition of ε suggests that G is independent of flow rate. The average droplet size and surface breakup efficiency would decrease with increasing We, but the rate of droplet emission would increase. Thus the breakup at prototypical flow rates would consist of smaller droplets of greater number but of equal mass flux compared to the scaled experiment. However, scaling based on the correlations may be inappropriate given the previously stated discrepancies between these investigations and the correlations.

PLIF results suggest that BL cutting changes the cross-sectional geometry of the flow, introducing sharp protrusions near the edges of the sheet that extend to the nominal free surface. Cutting also decreases the width (y-extent) of the jet at all downstream locations, reducing the width by almost 0.6 cm at $x/\delta = 25$ for $\dot{m}_{cut}/\dot{m}_{fl} = 1.9\%$. Calculations of beam standoff distances will probably need to be adjusted for streamwise variations in the cross-sectional shape of a slab jet, which continuously evolves from the original rectangular cross-section.

Equivalent number densities from the breakup of a single turbulent liquid sheet indicate that the hydrodynamic source term may be a significant design issue for thick liquid protection. For the standard flow conditioner configuration, "cutting" 1.0% of the total flow rate from each side of the jet will already meet the proposed upper limit of $N = 6\times10^{21}$ m^{-3} [Ref. 8]. Removing more fluid does not appear to significantly improve surface smoothness, but can be used to further reduce the number density of drops in the reactor chamber as required by new driver or target designs.

ACKNOWLEDGMENTS

REFERENCES

[1] R.W. MOIR, "The High-Yield Lithium-Injection Fusion-Energy (HYLIFE)-II Inertial Fusion Energy (IFE) Power Plant Concept and Implications for IFE," *Phys. Plasmas* **2**, 2447 (1995).

[2] S.P. LIN and R.D. REITZ, "Drop and Spray Formation from a Liquid Jet," *Annu. Rev. Fluid Mech.*, **30**, 85-105 (1998).

[3] K.A. SALLAM, Z. DAI and G.M. FAETH, "Liquid Breakup at the Surface of Turbulent Round Liquid Jets in Still Gases," *Int. J. of Multiphas. Flow*, **28**, 427-449 (2002).

[4] P.K. WU, R.F. MIRANDA, and G.M. FAETH, "Effects of Initial Flow Conditions on Primary Breakup of Nonturbulent and Turbulent Round Liquid Jets," *Atomization Spray*, **5**, 175-196 (1995).

[5] T. KARASAWA, M. TANAKA, K. ABE, S. SIGA, and T. KURABAYASHI, "Effects of Nozzle Configuration on the Atomization of a Steady Spray," *Atomization Spray*, **2**, 411-426 (1992).

[6] S.G. DURBIN, M. YODA, S.I. ABDEL-KHALIK, D.L. SADOWSKI and T.P. KOEHLER, "Assessment and Control of Primary Turbulent Breakup of Thick Liquid Sheets in IFE Reactor Cavities—The 'Hydrodynamic Source Term'," *Fusion Sci. Technol.*, To Appear (2005).

[7] S.G. DURBIN, T.P. KOEHLER, J.J.R. REPERANT, M. YODA, S.I. ABDEL-KHALIK and D.L. SADOWSKI, "Surface Fluctuation Analysis for Turbulent Liquid Sheets," *Fusion Sci. Technol.*, **45**, 1 (2004).

[8] R. PETZOLDT, B. RICKMAN, D. GOODIN and L. BROWN, "Heavy Ion Fusion Target Materials Selection and Removal of Tungsten Carbide from Flibe," Presented at ARIES-IFE Quarterly Meeting, Atlanta, GA (2003).

[9] S.G. DURBIN, M. YODA, and S.I. ABDEL-KHALIK, "Flow Conditioning Design in Thick Liquid Protection," *Fusion Sci. Technol.*, To Appear (2005).